




Effect of grain size distribution on the acoustic nonlinearity parameter

Cite as: J. Appl. Phys. **127**, 185102 (2020); <https://doi.org/10.1063/1.5119760>

Submitted: 15 July 2019 . Accepted: 25 April 2020 . Published Online: 08 May 2020

Saju T. Abraham , S. Shivaprasad , C. R. Das, S. K. Albert, B. Venkatraman, and Krishnan Balasubramaniam 



View Online



Export Citation



CrossMark

ARTICLES YOU MAY BE INTERESTED IN

[Janus nanoparticle synthesis: Overview, recent developments, and applications](#)

Journal of Applied Physics **127**, 170902 (2020); <https://doi.org/10.1063/5.0003329>

[Decoupling of Gd-Cr magnetism and giant magnetocaloric effect in layered honeycomb tellurate \$\text{GdCrTeO}_6\$](#)

Journal of Applied Physics **127**, 173902 (2020); <https://doi.org/10.1063/5.0006592>

[Electron dynamics in low pressure capacitively coupled radio frequency discharges](#)

Journal of Applied Physics **127**, 181101 (2020); <https://doi.org/10.1063/5.0003114>

Lock-in Amplifiers
up to 600 MHz



Effect of grain size distribution on the acoustic nonlinearity parameter

Cite as: J. Appl. Phys. 127, 185102 (2020); doi: 10.1063/1.5119760

Submitted: 15 July 2019 · Accepted: 25 April 2020 ·

Published Online: 8 May 2020



View Online



Export Citation



CrossMark

Saju T. Abraham,^{1,a)} S. Shivaprasad,² C. R. Das,¹ S. K. Albert,¹ B. Venkatraman,¹
and Krishnan Balasubramaniam²

AFFILIATIONS

¹Homi Bhabha National Institute, Indira Gandhi Centre for Atomic Research, Kalpakkam 603 102, Tamil Nadu, India

²Centre for Non-Destructive Evaluation, Indian Institute of Technology, Chennai 600 036, India

^{a)}Author to whom correspondence should be addressed: sajuta@igcar.gov.in

ABSTRACT

The effect of grain size distribution on the measured acoustic nonlinearity of polycrystalline engineering materials is investigated. Results are provided for two austenitic stainless steel materials with comparable mean grain sizes and distinct distribution widths assuming equiaxed grains and random crystallographic orientation. The distribution width is shown to influence the nonlinearity parameter considerably. On the material with a wider distribution, a reduced nonlinearity was noted, and comparable trends were also noted for different frequencies investigated. The results predict that the existing models that account for only the mean grain size when characterizing material degradations need to be modified more comprehensively to include the role of grain size distribution.

Published under license by AIP Publishing. <https://doi.org/10.1063/1.5119760>

I. INTRODUCTION

Uniform grain size distribution is a prerequisite for achieving consistent mechanical, physical, and chemical properties in engineering polycrystalline materials,¹ which also influences grain growth kinetics² and corrosion behavior.³ However, processes such as annealing or cold working introduce heterogeneity to this distribution, and hence design specifications come into force. Heterogeneous grain size distribution has a measurable impact on the mechanical properties as both strength and toughness increases with reducing grain size.⁴ Therefore, accurate evaluation of the grain size distribution is essential to predict the mechanical properties unambiguously. Optical and electron microscopy analyses are traditionally being employed to determine the grain size and its distribution, which are essential tools for all metallurgists.^{5,6} Though these methods provide extensive and accurate details, they are constrained by their destructive nature as well as laboratory confinement and time-consuming procedures for specimen preparation. In this context, non-destructive evaluation (NDE) methods find wide applications as they do not require tedious preparation of specimens and are being used during manufacture, processing, or in service on large industrial components. The ultrasonic technique is the most widely used among different NDE methods due to its high sensitivity, low operating costs, faster evaluation capabilities, and suitability to be applied on

any material. This technique is also well known to be used during the in-service inspection in order to detect the development and extension of service induced defects and assesses their acceptance as well as service life of the component.

In fact, traditional pulse-echo based ultrasonic techniques⁷ are highly sensitive to defects whose dimensions exceed a wavelength, whereas they are less sensitive to changes in microstructure. In such situations, ultrasonic velocity⁸ and attenuation⁹ measurements would be a better choice because they resemble the variations in the microstructure. However, only a trivial variation in ultrasonic velocity was observed with a measurable variation in grain size.^{8,10,11} Meanwhile, the power-law dependency¹² on the frequency (f) and the grain size (D) makes the attenuation more profound than the velocity variations.⁸ Attenuation measurements, however, have limited response to the phase changes in materials¹⁰ and the requirements of multiple reflections restrict high-frequency measurements on coarse-grained and thick materials. These limitations are overwhelmed using nonlinear ultrasonic (NLU) methods, which are considered to be very sensitive to the microstructural changes compared to the attenuation and velocity measurements.¹³ The NLU methods measure the acoustic nonlinearity parameter that is related to the lattice discontinuities in the crystalline solid and find excellent use in characterizing single crystal^{14,15} and

polycrystalline¹⁶ materials as well as in various mechanisms of materials processing¹⁷⁻²⁶ and microstructural degradation.²⁷⁻³³

The one-dimensional elastic wave equation in a medium with quadratic nonlinearity can be written as

$$\frac{\partial^2 u}{\partial t^2} = v^2 \left[1 - \beta^{lat} \frac{\partial u}{\partial x} \right] \frac{\partial^2 u}{\partial x^2}, \quad (1)$$

where v is the longitudinal velocity and β^{lat} is the intrinsic nonlinearity parameter induced by the elastic constants of the crystallites defined as^{34,35}

$$\beta^{lat} = - \left(\frac{k_3}{k_2} + 3 \right), \quad (2)$$

with k_2 and k_3 corresponding to the linear combinations of second-order and third-order elastic constants, respectively. In a single-phase polycrystalline elastic medium, the grain boundary dislocations introduce excess nonlinearity (β^{ex}) in addition to the intrinsic nonlinearity of the crystallites. Therefore, the effective nonlinearity parameter, β , of such a medium is the summation of β^{ex} and β^{lat} and the medium is termed as anisotropic. A monochromatic elastic waveform gets distorted as it propagates through an anisotropic medium and generates harmonics of the fundamental frequency. The nonlinearity parameter of the medium is related to the amplitudes of the fundamental and harmonic components. For experimental simplicity, β is defined as²⁷

$$\beta = \frac{8 A_2}{k^2 x A_1^2}, \quad (3)$$

with A_1 and A_2 corresponds to the amplitudes of the fundamental and second harmonic components, respectively, $k = \omega/c$ is the wave vector of the input wave of angular frequency ω and velocity c , and x is the propagation distance. In an anisotropic material, a monochromatic sinusoidal plane wave of frequency ω and amplitude A_1

- a. encounters attenuation losses during propagation and
- b. the second harmonic wave of frequency 2ω with amplitude A_2 is produced from the nonlinear interactions and, at the same time, its amplitude decreases due to the attenuation effects.

This implies that A_1 and A_2 get modified non-proportionately as³⁶

$$A_1 = (A_1)_0 e^{-\alpha_1 x}, \quad (4)$$

$$A_2 = \frac{1}{8} \beta_0 k^2 (A_1)_0^2 \left[\frac{e^{-2\alpha_1 x} - e^{-\alpha_2 x}}{\alpha_2 - 2\alpha_1} \right], \quad (5)$$

where α_i are the coefficients of attenuation ($i = 1$ for fundamental and $i = 2$ for second harmonic), β_0 is the material nonlinearity where the attenuation effects are not considered, and $(A_1)_0$ is the amplitude of the fundamental wave at $x = 0$. Equations (4) and (5) accounted for the attenuation of elastic waves as a combined effect of scattering and absorption. Scattering results from the fact that

the material is not strictly homogeneous whereas the absorption arises from the dislocation damping and internal friction. But, scattering losses are orders of magnitude higher than that due to absorption and hence microstructural characterization of engineering materials using ultrasonic methods is focused mainly on the scattering mechanisms. Therefore, growth of the second harmonic amplitude due to the nonlinear interactions as well as the attenuation losses to A_1 and A_2 during their propagation regulate the value of measured β . Substituting Eqs. (4) and (5) in Eq. (3) yields

$$\beta = \beta_0 \left[\frac{1 - \exp[-(\alpha_2 - 2\alpha_1)x]}{(\alpha_2 - 2\alpha_1)x} \right]. \quad (6)$$

According to Eq. (6), the measured β is a modified version of the material nonlinearity β_0 by a term consisting of the material's attenuation coefficients, α_i . This term, given in the square bracket of Eq. (6), is henceforth denoted as β_{α_i} . The attenuation coefficient can be experimentally determined from the frequency spectrum of the first [$u_1(\omega)$] and second [$u_2(\omega)$] back-reflected waves in a simple pulse-echo method using the relation³⁷

$$\alpha_\omega = \frac{1}{2x} \ln \left[\frac{V_1(\omega)}{V_2(\omega)} R_T R_B \frac{D_2(\omega)}{D_1(\omega)} \right], \quad (7)$$

where $V_1(\omega)$ and $V_2(\omega)$ are the spectral amplitudes at frequency ω of $u_1(\omega)$ and $u_2(\omega)$, $D_1(\omega)$ and $D_2(\omega)$ are the Lommel diffraction corrections to $u_1(\omega)$ and $u_2(\omega)$, $R = (\rho_m c_{Lm} - \rho_w c_{Lw}) / (\rho_m c_{Lm} + \rho_w c_{Lw})$ defines the reflection coefficients at the top (R_T) and bottom (R_B) surfaces, c_{Lm} and c_{Lw} are the longitudinal velocity in material and water, and ρ_m and ρ_w are the density of material and water, respectively. Since the elastic wave attenuation in a material is a function of D and f , the coefficients of attenuation would be different for fundamental and harmonic components associated with an NLU measurement. Magnitude of this difference, therefore, influences the measured β according to Eq. (6).^{38,39}

In addition to the mean grain size, extensive studies have been carried out on the influence of grain size distribution on the attenuation of elastic waves,⁴⁰⁻⁴² but such an attempt has yet to be extended to the acoustic nonlinearity parameter. Previous studies that correlated the nonlinearity parameter with the microstructure used only the mean grain size to describe the entire microstructure.^{38,43,44} Nevertheless, the grain size in any polycrystalline material is distributed lognormally,⁴⁵ and the effect of such distribution on the nonlinearity parameter has to be considered for a reliable characterization of the microstructure. Thus, the purpose of this paper is to investigate the impact of grain size distribution on the measured acoustic nonlinearity parameter, which can be used to develop a generalized approach in characterizing grain size heterogeneity in polycrystalline materials.

II. MATERIALS AND METHODS

Two AISI grade 304 austenitic stainless steel plates (designated as A and B) were used to investigate the effect of grain size distribution on the measured acoustic nonlinearity parameter. They were subjected to similar hot rolling conditions and heat treatment

cycles. Specimens for metallography were prepared with each of dimension $10 \times 10 \times 4 \text{ mm}^3$ cut from these plates, polished to diamond finish and subjected to electrolytic etching in 60 wt. % HNO_3 solution for microscopy analysis. Images were obtained using an Olympus GX51 inverted optical microscope. The mean grain size (D_{mean}) and the standard deviation (σ) were measured using the line intercept method as described in ASTM standard E112. Twins were also considered when measuring the grain boundaries as it is a common practice in the ultrasonic characterization of microstructure.⁴⁶

Specimens for nonlinear ultrasonic measurements were cut from these plates and machined to have a uniform surface finish of $6 \mu\text{m}$ and plane parallelism with thickness of $10 \pm 0.01 \text{ mm}$. Transmitter (T_x) and receiver (R_x) transducers of three frequency combinations, 2.25 MHz–4.5 MHz, 5.0 MHz–10.0 MHz, and 7.5 MHz–15.0 MHz, were used for nonlinear measurements. The measurements were carried out separately for each pair (T_x – R_x) of transducers aligned coaxially on opposite faces of the specimens. An RF tone burst of duration $2.6 \mu\text{s}$ was sent through the T_x using a computer-controlled high power ultrasonic pulser-receiver (RITEC RAM-5000 SNAP) system. The material response received through the corresponding R_x was fed to a digital storage oscilloscope (DSO) where it was converted into ASCII format for spectral analysis. The material response was collected at 20 different locations in each specimen for 6 different power levels of the SNAP system. A large number of measurements ensured the repeatability and statistical averaging of the measurement uncertainties. Amplitudes of the fundamental (A_1) and second harmonic (A_2) components were measured from the frequency spectrum of the received signals and used to calculate the nonlinearity parameter.

Subsequently, the specimens were immersed in a water bath for measuring the elastic wave attenuation at the ultrasonic frequencies used in NLU measurements. Unfocused immersion transducers of central frequency 2.25 MHz, 5.0 MHz, 10.0 MHz, and 15.0 MHz were excited individually using a JSR make DPR300 pulser-receiver, and the ultrasound beam was impinged on the specimen surface in the pulse-echo mode. The specimens were kept in the far-field of the transducers at which the water column height between the transducer face and the specimen surface was greater than r^2/λ_w , where r is the radius of the transducer and λ_w is the wavelength in water. Care has been taken to keep the surface of the specimen normal to the ultrasound beam. First and second back-reflected signals were stored in a DSO and the frequency-dependent attenuation was calculated from their spectral amplitudes using Eq. (7).

III. RESULTS AND DISCUSSIONS

A. Microstructure

The grain size in specimen A was measured to be within a range from $12 \mu\text{m}$ to $110 \mu\text{m}$ and that in B ranges from $8 \mu\text{m}$ to $124 \mu\text{m}$. Considering the lognormal distribution of grain sizes in polycrystalline materials, the logarithmic mean (D_{mean}) and the standard deviation (σ) in the given specimens were measured to be $D_{mean}^A = 3.7401 \mu\text{m}$, $\sigma^A = 0.45$ and $D_{mean}^B = 3.7375 \mu\text{m}$, $\sigma^B = 0.52$, where the superscript denotes the specimen. The probability distribution function (PDF) of the grain size is represented as histograms

fitted with lognormal distribution curves in Fig. 1. The presence of larger grains in specimen B is evident in the histogram. A careful observation of Fig. 1 shows that the fitted lognormal distribution function did not envelope the real distribution of grain sizes completely.

B. Nonlinearity parameter

A typical time domain output signal from the specimen A for the transducer combination of 5.0 MHz–10.0 MHz and the corresponding Fourier spectrum are shown in Figs. 2(a) and 2(b),

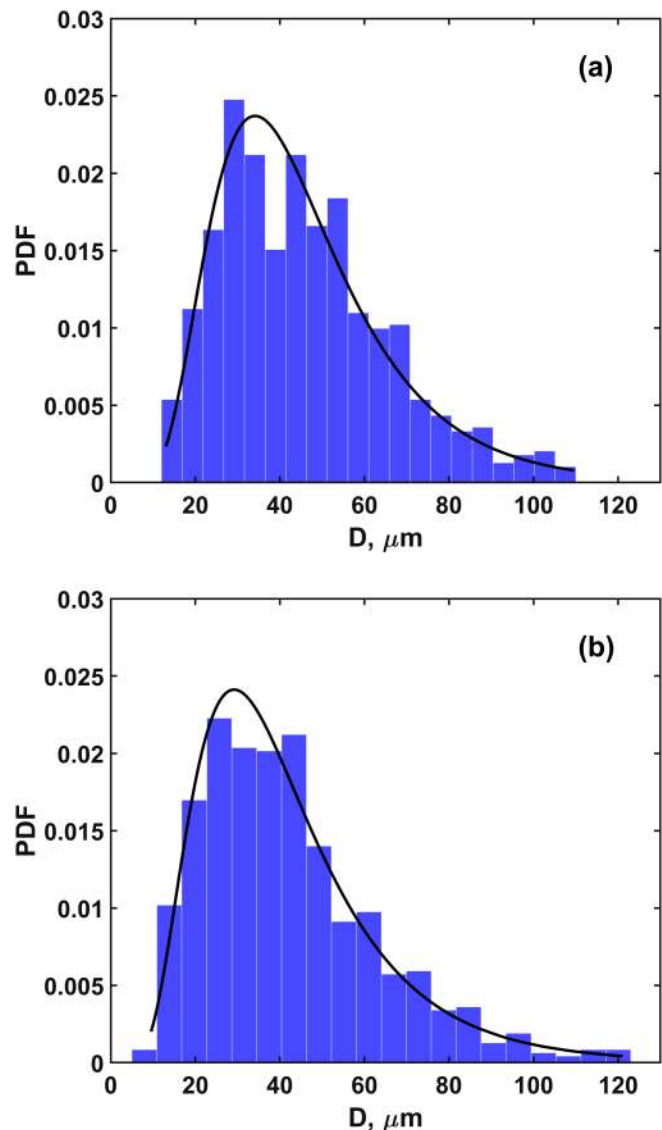


FIG. 1. Grain size distribution in the specimens with (a) $\sigma = 0.45$ and (b) $\sigma = 0.52$ presented as histograms with fitted curves for lognormal distribution.

respectively. Amplitudes of the fundamental (A_1) and the second harmonic (A_2) components were measured and the A_2 vs A_1^2 graph is plotted in Fig. 2(c) with a linear regression fit for six input power levels of the SNAP system. Similar trends were also observed for other transducer combinations: 2.25 MHz–4.5 MHz and 7.5 MHz–10.0 MHz. The slope of the A_2 vs A_1^2 graph is a direct representation of the nonlinear response of the material and hence the non-linearity parameter calculated from these slopes would characterize the microstructure. Therefore, in order to compare the material's nonlinear response with respect to different input frequencies, it would be convenient not considering the frequency term embedded

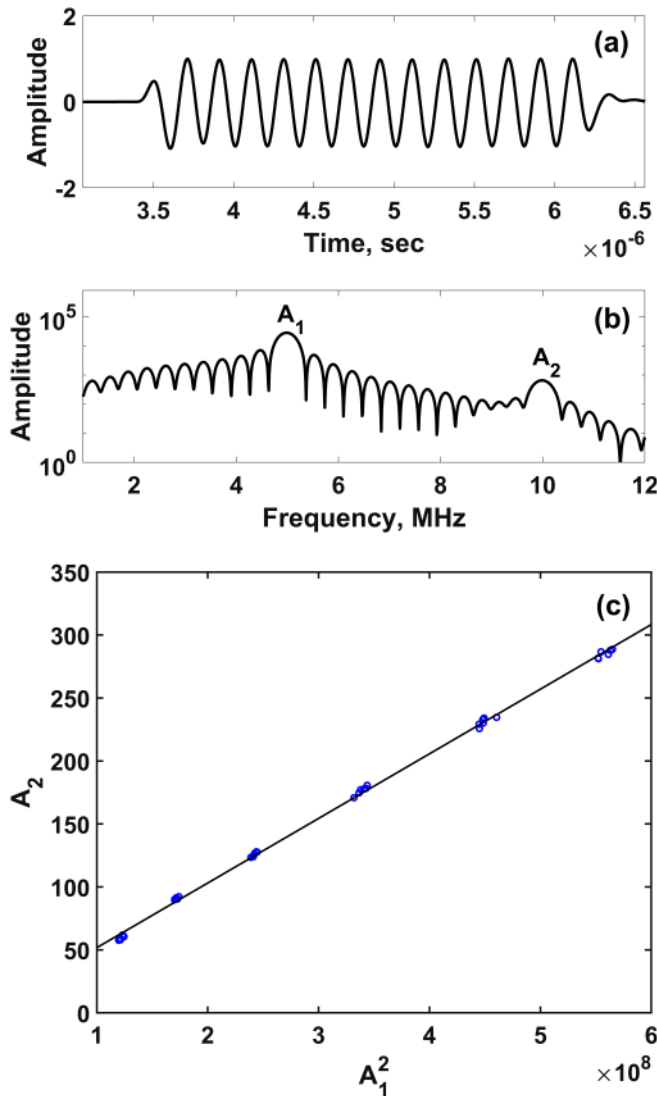


FIG. 2. (a) Typical time domain signal received from the specimen A, (b) corresponding Fourier spectrum, and (c) the A_2 vs A_1^2 graph fitted with linear regression for all six power levels and for a number of measurements.

in Eq. (3) as it is not an inherent material property.⁴³ Hence, the β plotted hereafter represents the A_2/xA_1^2 , which is also accounted for the thickness variations (albeit slightly) with location. It should be noted that the A_1^2 , which happens to be in the denominator of Eq. (3) is several orders of magnitude higher than A_2 . Hence, any change in A_1 , for example, due to the attenuation of the fundamental wave in the material, can significantly affect the measured β in comparison with a similar change in A_2 as it is being at the numerator.^{38,39} The measured β was normalized with that of the fused silica of the same thickness by $\beta_{norm} = \beta_{m,\omega_i} / \beta_{s,\omega_i}$, where the subscript m stands for the specimen A or B, s stands for silica, and ω_i represents the input applied frequency. Fused silica was selected as the reference material for normalization because of its isotropic nature to the acoustic wavelengths used and consistency in the absolute β value within the range of 11–14 as reported.⁴⁷ Such normalization would remove nonlinearities from other sources, such as instrumental or experimental and can also be standardized. The β_{norm} for the given specimens is plotted in Fig. 3. An obviously higher nonlinearity was observed for the specimen with smaller distribution in grain size.

Considering the equiaxed grains and random crystallographic orientation, the difference in β_{norm} among the specimens with comparable mean grain sizes can be explained on account of the difference in harmonic generation due to varying grain size distribution. Most prominent sources of harmonics in single-phase polycrystalline materials are the grain boundaries. A grain boundary is an array of edge dislocations where localized strain is high. The acoustic nonlinearity of an infinite array of dislocation dipoles is written as⁴⁸

$$\beta^{dis} = \Lambda b^2 \frac{c_2}{c_1^4} \Omega R^3 (1 - \nu)^3 \left(\frac{\sigma}{\mu} \right), \quad (8)$$

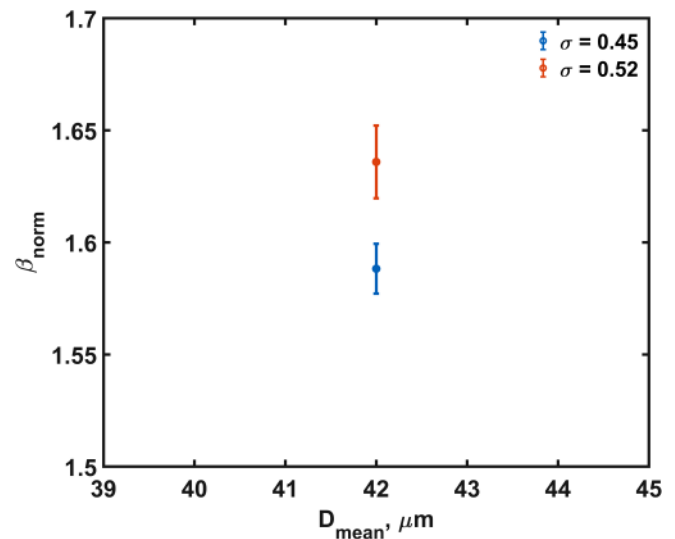


FIG. 3. β of the given specimens for an input frequency of 5 MHz normalized to that of the fused silica.

where Λ is the dislocation dipole density, b is the Burgers vector, c_1 and c_2 are constants, Ω is the orientation factor between the applied and the measured strain, R is the orientation factor between the applied stress and the resolved shear stress, ν is Poisson's ratio, h is the dislocation spacing, σ is the applied stress, and μ is the shear modulus. This equation implies that larger the dislocation density (Λ), higher would be the acoustic nonlinearity. Therefore, a higher value of β can be expected from the specimen with more numbers of smaller grains.^{38,43} This implies that the distribution of grain size has a vital role in the magnitude of measured β .

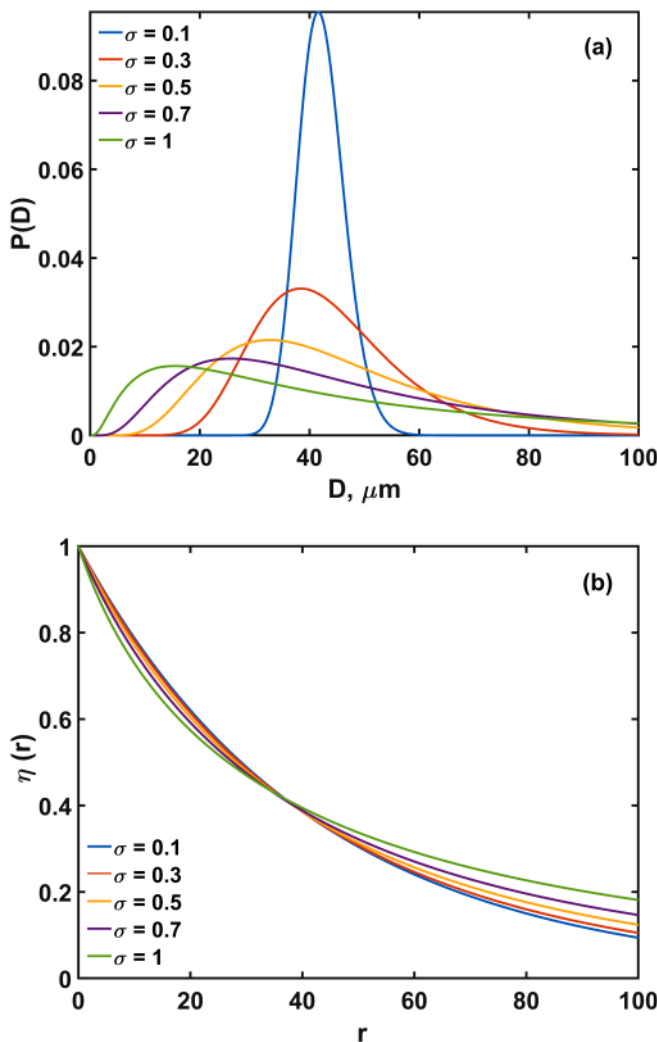


FIG. 4. (a) Probability distribution for constant mean, $D_{mean} = 42 \mu\text{m}$, and varying distribution widths ($\sigma = 0.1, 0.3, 0.5, 0.7, 1.0$) and (b) the corresponding spatial correlation function.

In a polycrystalline material, the probability distribution function $P(D)$ of the grain sizes (D) is defined as

$$P(D) = \frac{1}{D\sigma\sqrt{2\pi}} \exp\left[-\frac{\ln^2(D/\bar{D})}{2\sigma^2}\right], \quad (9)$$

where the median of the distribution $\bar{D} = \exp\mu$, which relates to the volumetric mean of the distribution $\bar{D} = \bar{D} \exp(\sigma^2/2)$, where σ is the logarithmic distribution width, and μ is the mean of the normal distribution. For a continuous lognormal distribution of grain sizes D , the spatial correlation function, describing the probability that two points at a correlation distance (r) fall in the same grain, may be written as⁴⁰

$$\eta(r) = \int_0^\infty P(D) \exp\left(-\frac{r}{D}\right) dD. \quad (10)$$

$P(D)$ is plotted in Fig. 4(a) for a constant \bar{D} and varying σ , and the corresponding $\eta(r)$ is plotted in Fig. 4(b). $\eta(r)$ has a higher amplitude at larger r for broader distributions, which indicates the presence of bigger grains. The attenuation of longitudinal waves in a polycrystalline material with a grain size distribution is analytically shown as⁴⁰

$$\alpha_L = \frac{k_L^2 \pi}{4\rho^2 c_L^2} \int_0^\pi \tilde{\eta}(\theta_{ps}) M_1(\theta_{ps}) \sin \theta_{ps} d\theta_{ps}, \quad (11)$$

with

$$\tilde{\eta}(\theta_{ps}) = \int_0^\infty P(D) \frac{D^3}{\pi^2 [1 + D^2(k^2 + k_s^2 + 2kk_s \cos \theta_{ps})]^2} dD, \quad (12)$$

where $\tilde{\eta}(\theta_{ps})$ is the Fourier transform of the spatial correlation function, θ_{ps} is the scattering angle, M_1 is the autocorrelation function of the elastic constants for the corresponding incident and scattered wave modes of wave vectors k and k_s and k_L and c_L are the wavenumber and velocity of incident longitudinal waves, respectively. In the Rayleigh scattering regime where $kD \ll 1$, Eq. (12) becomes

$$\tilde{\eta}(\theta_{ps}) = \int_0^\infty P(D) \frac{D^3}{\pi^2} dD. \quad (13)$$

In a single-phase polycrystalline material, it may be assumed that the anisotropy in the bulk modulus vanishes considering the bulk modulus of a single crystallite of cubic symmetry is equal to that of a polycrystal containing the cubic crystallites.⁴⁹ Also, random orientations of single-phase crystallites imply statistical isotropy and homogeneity to the polycrystal. In this condition, the Eq. (11) reduces to⁴⁰

$$\alpha_L^R = \frac{1}{15} \frac{\bar{D}^3 k_L^4}{\rho^2 c_L^4} \exp\left(\frac{9\sigma^2}{2}\right) \times \left[\frac{672}{36} \mu + \frac{1344}{48} \frac{\mu c_L^5}{c_T^5} \right], \quad (14)$$

where $\mu = 3(C_{11} - C_{12} - 2C_{44})^2/175$ is the second-order anisotropy⁴⁹ in the shear modulus. The attenuation coefficients for a

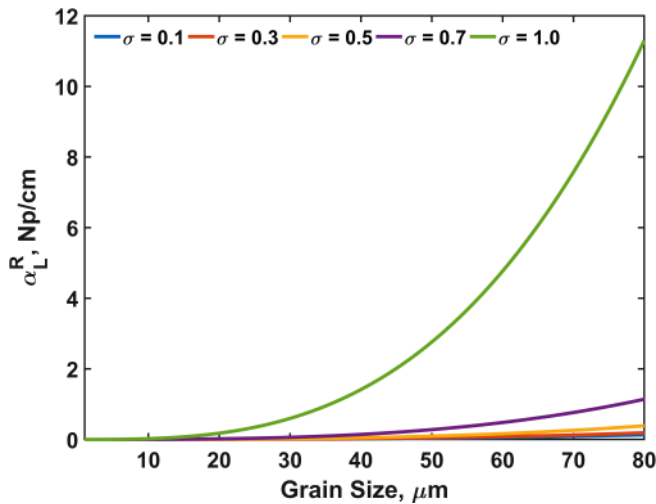


FIG. 5. Attenuation coefficients for different grain size distributions for an input monochromatic plane wave of frequency 5 MHz.

monochromatic plane wave of frequency 5 MHz and a set of distributions illustrated in Fig. 4(a) is plotted in Fig. 5. Assuming cubic symmetry of the material, the elastic constants were taken as $C_{11} = 200.4$ GPa, $C_{12} = 129.3$ GPa, and $C_{44} = 125.8$ GPa.⁵⁰ Figure 5 illustrates that the distribution of grain size influences the ultrasonic attenuation measurably. The deviations from the theoretical prediction by Stanke and Kino⁵¹ observed for the measured attenuation in low carbon steels,⁵² copper alloy,⁴⁶ nickel,⁴² and

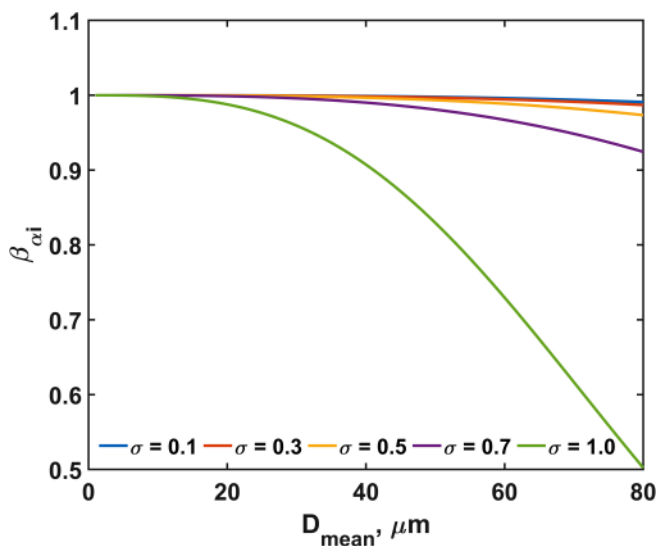


FIG. 6. β_{α_i} vs D_{mean} for different grain size distributions for an input frequency of 5 MHz.

titanium alloys^{41,53} were accounted for such distribution. Therefore, it is reasonable to conclude that σ can substantially influence the measured β as it is decided by the attenuation coefficients, α_i , according to Eq. (6). This influence, termed as β_{α_i} , is graphically exemplified in Fig. 6 for a wave of frequency 5 MHz.

The measured nonlinearity parameters for three different input frequencies were normalized to that of the fused silica and shown in Fig. 7(a). It is seen that an order $\beta_{2.25} > \beta_{5.0} > \beta_{7.5}$ (suffix corresponds to the applied frequency) is maintained, and in each case, the specimen with wider σ shows a relatively lower β consistently. The observed trend has similarity to Fig. 7(b) in which β_{α_i} is plotted for similar distribution widths and input

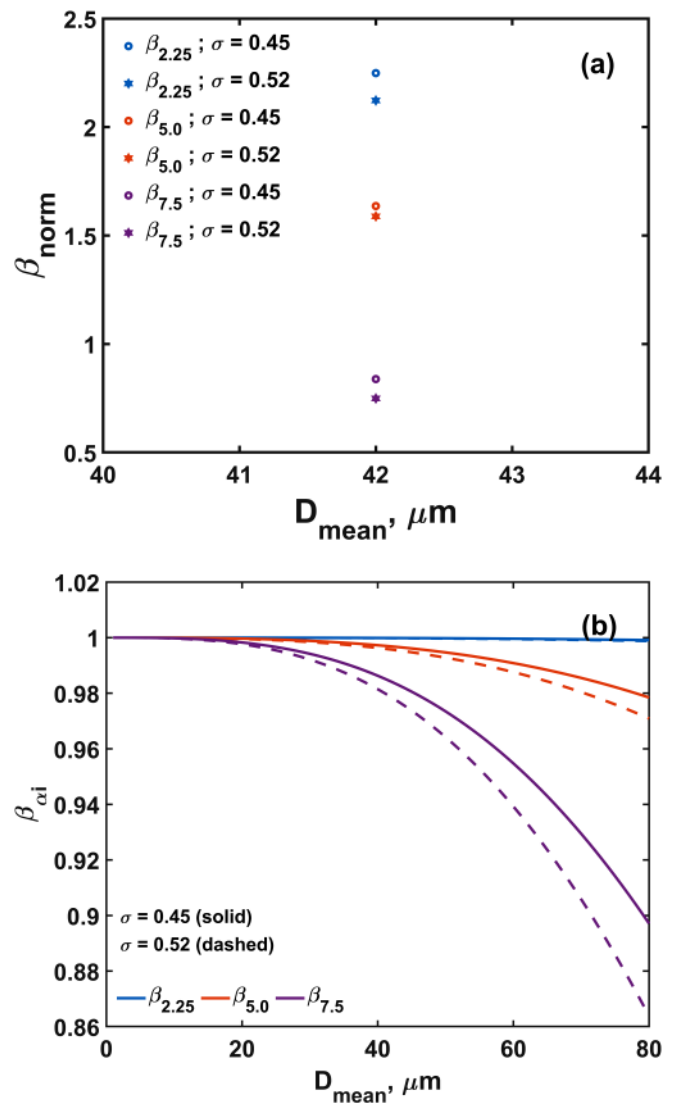


FIG. 7. (a) Normalized β for three input frequencies 2.25 MHz, 5.0 MHz, and 7.5 MHz showed the similar trend to the (b) numerical analysis.

frequencies. The drop in β (Fig. 7) with an increase in applied frequency is a consequence of the difference in the attenuation of A_1 and A_2 components. In a single-phase polycrystalline material, attenuation is predominantly due to grain boundary scattering and governed by the power-law relations¹² of D and f , which defines different scattering regimes described by a dimensionless number “ kD .” The Rayleigh-to-stochastic scattering transition condition $kD = 1$ in the given specimens occurs at the grain sizes $D_{2.25} = 410\mu\text{m}$, $D_{5.0} = 184\mu\text{m}$, and $D_{7.5} = 123\mu\text{m}$ where the suffix corresponds with the input frequency, whereas the scattering transition condition for the respective second harmonic components occur at $D_{4.5} = 205\mu\text{m}$, $D_{10.0} = 92\mu\text{m}$, and $D_{15.0} = 62\mu\text{m}$. This implies that, for the present materials in which the grain size

TABLE I. The grain distribution parameters contributing to the stochastic scattering of harmonic components.

A			B		
$\mu_{10.0}^s$	4.37		$\mu_{10.0}^s$	4.31	
$\sigma_{10.0}^s$	0.15		$\sigma_{10.0}^s$	0.19	
$V_{10.0}^s$	3.73		$V_{10.0}^s$	3.75	
$\mu_{15.0}^s$	4.59		$\mu_{15.0}^s$	4.62	
$\sigma_{15.0}^s$	0.07		$\sigma_{15.0}^s$	0.11	
$V_{15.0}^s$	16.50		$V_{15.0}^s$	19.65	

measured to be less than $124\mu\text{m}$, all input frequencies satisfy the Rayleigh scattering condition at which the attenuation coefficient varies as D^2f^4 . Meanwhile, the higher harmonic components of 10 MHz and 15 MHz are likely to undergo stochastic interactions with few grains. In such cases, the attenuation coefficient varies as Df^2 , which impose higher attenuation even if Rayleigh type interactions occur. The histogram representation of grains contributing to the stochastic scattering of 10 MHz (D_{10}^s) and 15 MHz (D_{15}^s) components is superimposed on the total distribution (TD) and illustrated in Fig. 8. The volume fraction (V_{ω}^s) and the corresponding logarithmic mean (μ_{ω}^s) and distribution width (σ_{ω}^s) in each stochastic scattering regime is determined and tabulated in Table I. These parameters decide the attenuation coefficients of the corresponding harmonic components. Higher the volume fraction (V_{ω}^s) and the applied frequency, higher will be the attenuation which results in $\alpha_{15\text{MHz}} > \alpha_{10\text{MHz}}$ leading to $A_2(15\text{MHz}) < A_2(10\text{MHz})$. Consequently, β drops with an increase in the applied frequency.

It can also be inferred from the experimental results [Fig. 7(a)] that the difference in β_{ω_i} with applied frequency ($\Delta\beta_{\omega_L-\omega_U} = \beta_{\omega_L} - \beta_{\omega_U}$, where ω_L and ω_U corresponds with the lower and higher input frequencies under consideration) exhibits

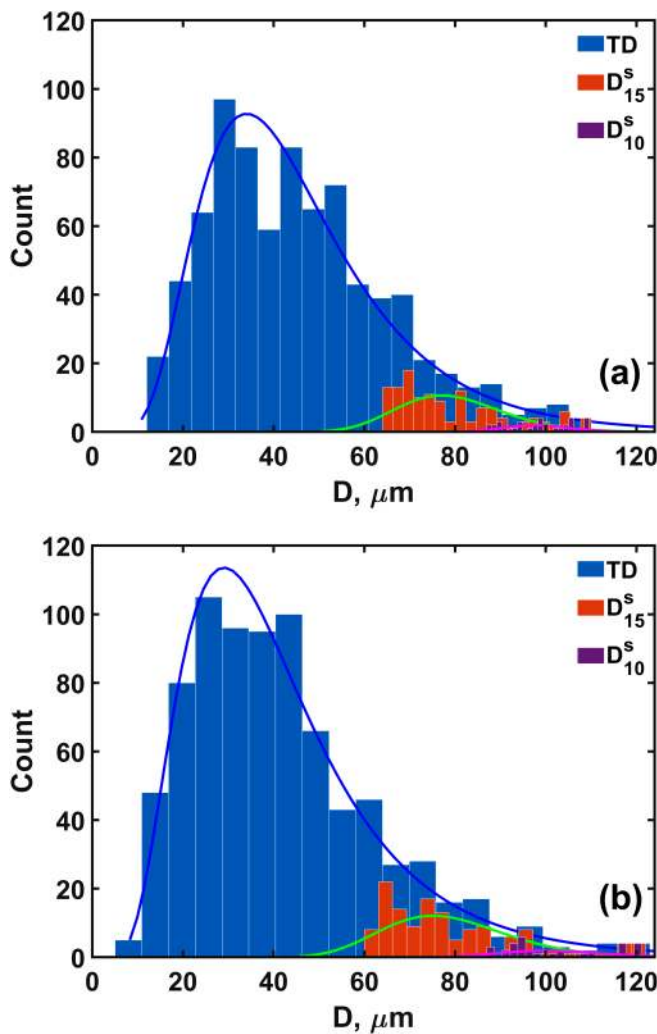


FIG. 8. Total grain size distribution (TD) superimposed with the distribution at the scattering regimes for 10 MHz (D_{10}^s) and 15 MHz (D_{15}^s) in specimens with (a) $\sigma = 0.45$ and (b) $\sigma = 0.52$.

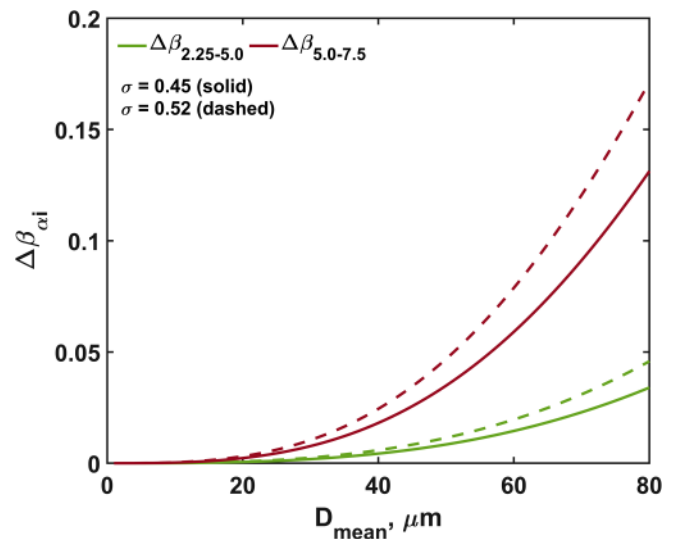


FIG. 9. Numerical results exhibits the relation $\beta_{2.25-5.0} < \beta_{5.0-7.5}$, which is also a function of the grain size distribution, σ .

the relation $\beta_{2.25-5.00} < \beta_{5.0-7.5}$, which bear a resemblance to Fig. 9 derived from the numerical results. As demonstrated by Abraham *et al.* for a set of annealed³⁸ and forged³⁹ microstructures, the relationship in $\Delta\beta_{\omega_1-\omega_2}$ and the order in β_{ω_1} observed in Fig. 7 will be maintained as long as the Rayleigh scattering condition is satisfied for all three input frequencies. Deviation from this behavior was used in characterizing microstructural heterogeneity in forgings with large dimensions.³⁹ Nevertheless, in this investigation on forgings³⁹ and the studies conducted on copper⁴³ and stainless steel,⁵⁴ the effect of grain size distribution on measured β was not adequately discussed. But, the findings in the present manuscript signify the importance of integrating the distribution of grain size in characterizing the microstructure using acoustic nonlinearity parameter.

C. Ultrasonic attenuation

The attenuation of harmonic components has been seen as playing a vital role in the behavior of the measured nonlinearity parameter. To substantiate the claims above, the attenuation of the frequency components used in the nonlinear measurements was determined from the immersion ultrasonic measurements. A typical time domain signal indicating the $u_1(\omega)$ and $u_2(\omega)$ for an excitation frequency 5 MHz and the corresponding frequency spectra are shown in Figs. 10(a) and 10(b), respectively. Frequency-dependent attenuation was measured over the range of frequencies within the full width at half maximum (FWHM) and the attenuation of the frequency components used in the nonlinear measurements are plotted in Fig. 11.

According to the classical scattering theory, a D^2f^4 dependency on the attenuation was expected for the mean grain sizes in

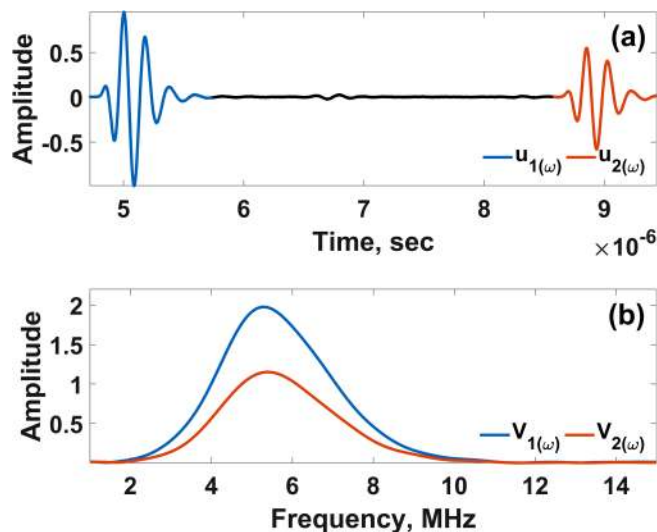


FIG. 10. (a) Typical time domain signal obtained for $\omega = 5$ MHz in the pulse-echo immersion mode shows the first [$u_1(\omega)$] and second [$u_2(\omega)$] back-reflected echoes and (b) the corresponding frequency spectra $V_1(\omega)$ and $V_2(\omega)$, respectively.

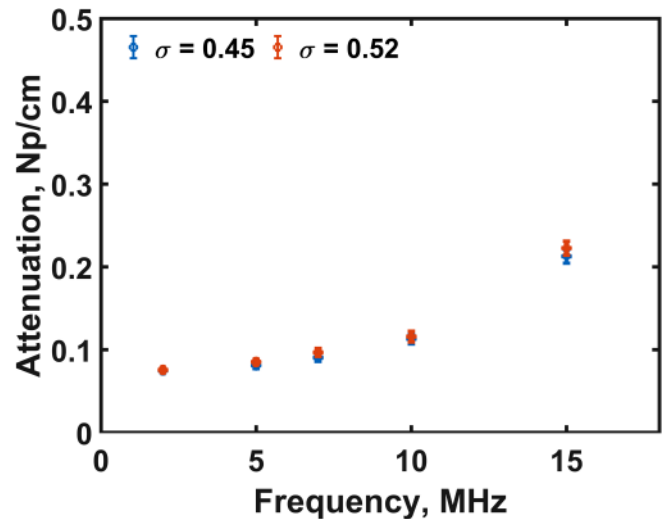


FIG. 11. Attenuation vs frequency for the given materials over the frequencies used in the nonlinearity measurement.

the Rayleigh scattering regime,^{55,56} but a deviation from this dependency was observed in Fig. 11. This is due to the distribution of the grain size in the microstructure, which is explained as follows. The classical D^2f^4 dependency in the Rayleigh regime and the Df^2 dependency in the stochastic regime is valid at the theoretical Rayleigh point defined as $kD = 0.1$ and at the stochastic point defined as $kD = 10$, respectively. In the Rayleigh-to-stochastic transition zone (kD varies from 0.1 to 10), the attenuation exhibits neither fourth-order nor quadratic dependency on f because of the simultaneous occurrence of the Rayleigh and stochastic scattering due to the coexistence of fine and coarse grains in the microstructure.^{37,46,51} In addition, the classical scattering theory was formulated based on the assumption that all grains have the same volume, and the grain size distribution is small. However, in real industrial components, the grain size distribution is lognormal with a significant fraction of larger grains. Attenuation due to stochastic interactions with larger grains is predominant even though there occurs Rayleigh scattering. Studies on low carbon steels⁵² and nickel⁴² reported that there can be a deviation in the order of dependency on f , which is attributed to the distribution of grain sizes. Arguelles and Turner⁴⁰ analytically demonstrated the influence of grain size distribution on attenuation and subsequently evaluated on titanium alloys.^{41,53} The kD values which were measured to be within 0.02–1.92 in the present investigation, extend from the classical Rayleigh scattering regime to the scattering transition zone. Therefore, the deviation in the power-law dependency observed in Fig. 11 is justified. Since the primary purpose of the present manuscript is to investigate the nonlinear response as a function of the distribution of grain size, the attenuation measurements were not explored in greater detail. Also, it should be emphasized at this point that a one-to-one comparison between the attenuation of ultrasonic waves measured in the linear regime and that of the harmonic components produced as a result of

nonlinear interactions is not possible. This is because the harmonic components are produced inside the material as the wave propagates through it and not from the source at the entry.⁵⁷ However, a simultaneous measurement of attenuation and the nonlinearity parameter is possible using a delicate transfer function method,⁵⁸ but it was not attempted as it does not fall within the scope of the present manuscript. Meanwhile, it was observed that the specimen with higher grain size distribution showed relatively higher attenuation, which is in line with the theory and literature.⁴⁰ It is evident from the conventional measurements plotted in Fig. 11 that the attenuation increases with frequency that substantiates the decrease in β as shown in Fig. 7(a).

In summary, this manuscript demonstrates that the grain size distribution has a considerable impact on the measured acoustic nonlinearity parameter and further supported through numerical model results. Although the results discussed here are in the context of the Rayleigh scattering regime, a similar influence of the distribution on β is expected for other scattering regimes also. Characterization of a polycrystalline material using the mean grain size alone is inadequate, and the distribution of grain size should be considered in order to interpret the findings correctly. This fact was not addressed while reporting the correlation between the nonlinearity parameter and the grain sizes in copper⁴³ and stainless steel.^{38,39,54} The results in this manuscript have industrial relevance. As the size of the component increases, grain size variation occurs across the thickness.⁵⁹ The manufacturing practices may also lead to the development of prior austenite grain size variations across the dimensions resulting in changes in mechanical properties.⁶⁰ Methods of ultrasonic attenuation or velocity measurements are not useful in characterizing such changes. Though property variation can be evaluated with several destructive tests, such practices are costly and time-consuming and cannot be implemented on a finished product. In such cases, nonlinear ultrasonic testing would be an ideal choice due to its superior response toward the microstructural changes in contrast to the linear ultrasonic methods.¹³ However, most research in nonlinear ultrasonics accounts for only the mean grain size when characterizing material degradations. These models need to be modified more comprehensively to include the role of grain size distribution, which is crucial for reliable characterization of microstructural features that meet the design requirements. The findings presented here demand a detailed analytical study connecting the relationship between D_{mean} , σ , β_{ω_i} , and $\Delta\beta_{\omega_L-\omega_U}$.

IV. CONCLUSION

The effect of grain size distribution on the acoustic nonlinearity parameter is investigated in this paper. The numerical results were validated for two austenitic stainless steel materials with similar mean grain sizes but distinct distribution widths. It was found that the material with a wider distribution exhibited reduced nonlinearity. Results demonstrated the significance of considering the distribution width in characterizing the microstructural features from the nonlinear response of the material. This observation is vital for accurate characterization of the microstructure as the reliability of nonlinear measurements depends on the knowledge of the mean grain size as well as its distribution.

REFERENCES

- 1X. Yuan, L. Chen, Y. Zhao, H. Di, and F. Zhu, *Procedia Eng.* **81**, 143 (2014).
- 2B.-N. Kim, K. Hiraga, and K. Morita, *Mater. Trans.* **44**, 2239 (2003).
- 3S. Gollapudi, *Corros. Sci.* **62**, 90 (2012).
- 4S. Berbenni, V. Favier, and M. Berveiller, *Int. J. Plast.* **23**, 114 (2007).
- 5A. P. Day and T. E. Quedest, *J. Microsc.* **195**, 186 (1999).
- 6K. P. Mingard, B. Roebuck, E. G. Bennett, M. G. Gee, H. Nordenstrom, G. Sweetman, and P. Chan, *Int. J. Refract. Met. Hard Mater.* **27**, 213 (2009).
- 7M. V. Felice and Z. Fan, *Ultrasonics* **88**, 26 (2018).
- 8P. Palanichamy, A. Joseph, T. Jayakumar, and B. Raj, *NDT&E Int.* **28**, 179 (1995).
- 9M. Aghaie-Khafri, F. Honarvar, and S. Zanganeh, *J. Nondestruct. Eval.* **31**, 191 (2012).
- 10A. Kumar, K. Laha, T. Jayakumar, K. B. S. Rao, and B. Raj, *Metall. Mater. Trans. A Phys. Metall. Mater. Sci.* **33**, 1617 (2002).
- 11M. Vasudevan and P. Palanichamy, *J. Mater. Eng. Perform.* **11**, 169 (2002).
- 12E. P. Papadakis, *J. Acoust. Soc. Am.* **37**, 711 (1965).
- 13P. B. Nagy, *Ultrasonics* **36**, 375 (1998).
- 14M. A. Breazeale and J. Ford, *J. Appl. Phys.* **36**, 3486 (1965).
- 15W. B. Gauster and M. A. Breazeale, *Phys. Rev.* **168**, 655 (1968).
- 16M. A. Breazeale and D. O. Thompson, *Appl. Phys. Lett.* **3**, 77 (1963).
- 17J. H. Cantrell, *J. Appl. Phys.* **100**, 063508 (2006).
- 18A. Kumar, R. R. Adharapurapu, J. W. Jones, and T. M. Pollock, *Scr. Mater.* **64**, 65 (2011).
- 19S. Baby, B. Nagaraja Kowmudi, C. M. Omprakash, D. V. V. Satyanarayana, K. Balasubramaniam, and V. Kumar, *Scr. Mater.* **59**, 818 (2008).
- 20J. S. Valluri, K. Balasubramaniam, and R. V. Prakash, *Acta Mater.* **58**, 2079 (2010).
- 21A. Metya, M. Ghosh, N. Parida, and S. Palit Sagar, *NDT&E Int.* **41**, 484 (2008).
- 22A. Viswanath, B. P. C. Rao, S. Mahadevan, T. Jayakumar, and B. Raj, *J. Mater. Sci.* **45**, 6719 (2010).
- 23A. Viswanath, B. P. C. Rao, S. Mahadevan, P. Parameswaran, T. Jayakumar, and B. Raj, *J. Mater. Process. Technol.* **211**, 538 (2011).
- 24A. Ruiz, N. Ortiz, A. Medina, J. Y. Kim, and L. J. Jacobs, *NDT&E Int.* **54**, 19 (2013).
- 25K. H. Matlack, J. J. Wall, J. Y. Kim, J. Qu, L. J. Jacobs, and H. W. Viehrig, *J. Appl. Phys.* **111**, 203 (2012).
- 26Y. Xiang, M. Deng, F.-Z. Z. Xuan, and C.-J. J. Liu, *NDT&E Int.* **44**, 768 (2011).
- 27S. T. Abraham, S. K. Albert, C. R. Das, N. Parvathavarthini, B. Venkatraman, R. S. Mini, and K. Balasubramaniam, *Acta Metall. Sin. (Engl. Lett.)* **26**, 545 (2013).
- 28J. H. Cantrell and W. T. Yost, *Appl. Phys. Lett.* **77**, 1952 (2000).
- 29C. Mondal, A. Mukhopadhyay, and R. Sarkar, *J. Appl. Phys.* **108**, 124910 (2010).
- 30A. Hikata, B. B. Chick, and C. Elbaum, *J. Appl. Phys.* **36**, 229 (1965).
- 31W. D. Cash and W. Cai, *J. Appl. Phys.* **109**, 014915 (2011).
- 32T. H. Lee and K. Y. Jhang, *NDT&E Int.* **42**, 757 (2009).
- 33J. Jiao, J. Sun, N. Li, G. Song, B. Wu, and C. He, *NDT&E Int.* **62**, 122 (2014).
- 34M. A. Breazeale, *Review of Progress in Quantitative Nondestructive Evaluation* (Springer, Boston, MA, 1990), pp. 1653–1660.
- 35J. H. Cantrell, *J. Appl. Phys.* **76**, 3372 (1994).
- 36J. H. Cantrell, in *Ultrasonic Nondestructive Evaluation: Engineering and Biological Material Characterization*, edited by T. Kundu (CRC Press, 2003), pp. 363–433.
- 37F. Zeng, S. R. Agnew, B. Raesinia, and G. R. Myneni, *J. Nondestruct. Eval.* **29**, 93 (2010).
- 38S. T. Abraham, S. Shivaprasad, N. Sreevidya, C. R. Das, S. K. Albert, B. Venkatraman, and K. Balasubramaniam, *Metall. Mater. Trans. A* **50**, 5567 (2019).
- 39S. T. Abraham, S. Shivaprasad, C. R. Das, S. K. Albert, B. Venkatraman, and K. Balasubramaniam, *Mater. Sci. Technol.* **36**, 699 (2020).

- ⁴⁰A. P. Arguelles and J. A. Turner, *J. Acoust. Soc. Am.* **141**, 4347 (2017).
- ⁴¹X. Bai, Y. Zhao, J. Ma, Y. Liu, and Q. Wang, *Materials* **12**, 102 (2019).
- ⁴²M. Norouzian, S. Islam, and J. A. Turner, *Ultrasonics* **102**, 106032 (2020).
- ⁴³R. S. Mini, K. Balasubramaniam, and P. Ravindran, *Exp. Mech.* **55**, 1023 (2015).
- ⁴⁴W. Li, B. Chen, X. Qing, and Y. Cho, *Metals* **9**, 271 (2019).
- ⁴⁵C. Núñez and S. Domingo, *Metall. Trans. A* **19**, 2937 (1988).
- ⁴⁶X.-G. Zhang, W. A. Simpson, J. M. Vitek, D. J. Barnard, L. J. Tweed, and J. Foley, *J. Acoust. Soc. Am.* **116**, 109 (2004).
- ⁴⁷D. C. Hurley and C. M. Fortunko, *Meas. Sci. Technol.* **8**, 634 (1997).
- ⁴⁸W. D. Cash and W. Cai, *J. Appl. Phys.* **111**, 074906 (2012).
- ⁴⁹C. M. Kube and A. N. Norris, *J. Acoust. Soc. Am.* **141**, 2633 (2017).
- ⁵⁰K. Benyelloul and H. Aourag, *Comput. Mater. Sci.* **67**, 353 (2013).
- ⁵¹F. E. Stanke and G. S. S. Kino, *J. Acoust. Soc. Am.* **75**, 665 (1984).
- ⁵²R. L. Smith, *Ultrasonics* **20**, 211 (1982).
- ⁵³F. Dong, X. Wang, Q. Yang, H. Liu, D. Xu, Y. Sun, Y. Zhang, R. Xue, and S. Krishnaswamy, *Scr. Mater.* **154**, 40 (2018).
- ⁵⁴S. Choi, J. Ryu, J.-S. Kim, and K.-Y. Jhang, *Metals* **9**, 1279 (2019).
- ⁵⁵E. P. Papadakis, *J. Appl. Phys.* **34**, 265 (1963).
- ⁵⁶E. P. Papadakis, *Int. Met. Rev.* **29**, 1 (1984).
- ⁵⁷T. Brunet, X. Jia, and P. A. Johnson, *Geophys. Res. Lett.* **35**, 2 (2008).
- ⁵⁸H. Jeong, D. Barnard, S. Cho, S. Zhang, and X. Li, *Ultrasonics* **81**, 147 (2017).
- ⁵⁹J. Sinczak, J. Majta, M. Glowacki, and M. Pietrzyk, *J. Mater. Process. Technol.* **80–81**, 166 (1998).
- ⁶⁰Y. Prawoto, N. Jasmawati, and K. Sumeru, *J. Mater. Sci. Technol.* **28**, 461 (2012).